ISSN 1674-1056
http://cpb.iphy.ac.cn
http://iopscience.iop.org/cpb
中国物理 B
Chinese Physics
中国物理
Chinese Physics B

Conductive property of $Zr_{0.1}Fe_{0.9}V_{1.1}Mo_{0.9}O_7$ with low thermal expansion

Xiaoke He(何小可), Heng Qi(戚恒), Qi Xu(徐启), Xiansheng Liu(刘献省), Lei Xu(许磊), Baohe Yuan(袁保合)

Citation: Chin. Phys. B . 2019, 28(5): 056501. **doi:** 10.1088/1674-1056/28/5/056501
Journal homepage: http://cpb.iphy.ac.cn; http://iopscience.iop.org/cpb

What follows is a list of articles you may be interested in

Alkyl group functionalization-induced phonon thermal conductivity attenuation in graphene nanoribbons

Caiyun Wang(王彩云), Shuang Lu(鲁爽), Xiaodong Yu(于晓东), Haipeng Li(李海鹏)
Chin. Phys. B . 2019, 28(1): 016501. **doi:** 10.1088/1674-1056/28/1/016501

Thermal conductivity of systems with a gap in the phonon spectrum

E Salamatov
Chin. Phys. B . 2018, 27(7): 076502. **doi:** 10.1088/1674-1056/27/7/076502

Thermal transport in phosphorene and phosphorene-based materials: A review on numerical studies

Yang Hong(洪扬), Jingchao Zhang(张景超), Xiao Cheng Zeng(曾晓成)
Chin. Phys. B . 2018, 27(3): 036501. **doi:** 10.1088/1674-1056/27/3/036501

Thermal conductivity of carbon nanotube superlattices: Comparative study with defective carbon nanotubes

Kui-Kui Zhou(周魁葵), Ning Xu(徐 宁), Guo-Feng Xie(谢国锋)
Chin. Phys. B . 2018, 27(2): 026501. **doi:** 10.1088/1674-1056/27/2/026501

Thermal transport in twisted few-layer graphene

Min-Hua Wang(王敏华), Yue-E Xie(谢月娥), Yuan-Ping Chen(陈元平)
Chin. Phys. B . 2017, 26(11): 116503. **doi:** 10.1088/1674-1056/26/11/116503

Conductive property of $Zr_{0.1}Fe_{0.9}V_{1.1}Mo_{0.9}O_7$ with low thermal expansion*

Xiaoke He(何小可)[1], Heng Qi(戚恒)[1], Qi Xu(徐启)[1], Xiansheng Liu(刘献省)[2,†], Lei Xu(许磊)[1], and Baohe Yuan(袁保合)[1,‡]

[1] North China University of Water Resources and Electric Power, Zhengzhou 450011, China
[2] Henan Key Laboratory of Photovoltaic Materials, Henan University, Kaifeng 475004, China

(Received 6 December 2018; revised manuscript received 18 March 2019; published online 4 April 2019)

Low thermal expansion materials are mostly ceramics with low conductive property, which limits their applications in electronic devices. The poor conductive property of ceramic ZrV_2O_7 could be improved by bi-substitution of Fe and Mo for Zr and V, accompanied with low thermal expansion. $Zr_{0.1}Fe_{0.9}V_{1.1}Mo_{0.9}O_7$ has electrical conductivity of 8.2×10^{-5} S/cm and 9.41×10^{-4} S/cm at 291 K and 623 K, respectively. From 291 K to 413 K, thermal excitation leads to the increase of carrier concentration, which causes the rapid decrease of resistance. At 413–533 K, the conductivity is unchanged due to high scattering probability and a slowing increase of carrier concentration. The conductivity rapidly increases again from 533 K to 623 K due to the intrinsic thermal excitation. The thermal expansion coefficient of $Zr_{0.1}Fe_{0.9}V_{1.1}Mo_{0.9}O_7$ is as low as 0.72×10^{-6} K^{-1} at 140–700 K from the dilatometer measurement. These properties suggest that $Zr_{0.1}Fe_{0.9}V_{1.1}Mo_{0.9}O_7$ has attractive application in electronic components.

Keywords: low thermal expansion, conductivity, thermal excitation, electric impedance

PACS: 65.40.De, 84.32.Ff, 73.50.Gr **DOI:** 10.1088/1674-1056/28/5/056501

1. Introduction

Metal materials have excellent conductivity, but their thermal expansion property could induce thermal stress and even function failure. Meanwhile, ceramic materials have low thermal expansion coefficients but their conductivities are usually poor. Recent investigations suggest that negative thermal expansion materials could be used to prepare low thermal expansion materials by partial ion substitution, doping, or compounding with positive thermal expansion materials,[1–3] which could also result in high conductivity.[4–8]

ZrV_2O_7 is one of the isotropic negative thermal expansion materials but its negative thermal expansion is only present after a phase transition.[9] P^{5+} ion has been used to substitute V^{5+} in ZrV_2O_7 to decrease the phase transition temperature and realize low thermal expansion. $ZrV_{2-x}P_xO_7$ ($0 \le x \le 1$) showed lower phase transition temperature at 340 K for x = 0.4.[10] The heterovalent ion substitution of Mo^{6+} or W^{6+} for V^{5+} in ZrV_2O_7 could not reduce the phase transition temperature obviously.[11,12] Dual-ion substitutions of Cu^{2+}/P^{5+} or Fe^{3+}/P^{5+} for Zr^{4+}/V^{5+} in ZrV_2O_7 have also been investigated but it is difficult to reach a high solubility of the dopants.[13,14] However, dual-ion Fe^{3+}/Mo^{6+} or Al^{3+}/Mo^{6+} for Zr^{4+}/V^{5+} in ZrV_2O_7 could lead to a low thermal expansion material.[15,16] Even near zero thermal expansion can be obtained ($Zr_{0.1}Fe_{0.9}V_{1.1}Mo_{0.9}O_7$) by dual-ion substitutions of Fe^{3+}/Mo^{6+} for Zr^{4+}/V^{5+} in ZrV_2O_7.[15]

ZrV_2O_7 has poor conductivity at room temperature (RT), which is increased with increasing temperature ($\sigma = 3.56 \times 10^{-3}$ S/cm at 573 K).[13,17] The introduction of Cs in ZrV_2O_7 could enhance the ionic conductivity. Charge transport in VO_4 could provide the observed high ionic conductivity.[18,19] In this paper, dual-ion substitutions of Fe^{3+}/Mo^{6+} for Zr^{4+}/V^{5+} in ZrV_2O_7 are investigated to increase the conductivity of ZrV_2O_7. $Zr_{0.1}Fe_{0.9}V_{1.1}Mo_{0.9}O_7$ is found with electrical conductivity $\sigma = 8.2 \times 10^{-5}$ and 9.41×10^{-4} S/cm at 291 K and 623 K, and activation energy $E_a = 0.160$ eV and 0.233 eV for 291–413 K and 533–623 K, calculated from the Arrhenius plots for the total conductivity.

2. Experiments

$Zr_{0.1}Fe_{0.9}V_{1.1}Mo_{0.9}O_7$ was synthesized by a solid state method with raw materials Fe_2O_3, ZrO_2, MoO_3, and V_2O_5. The raw materials were mixed according to stoichiometric amounts of $Zr_{0.1}Fe_{0.9}V_{1.1}Mo_{0.9}O_7$ (with excess 5 mol% V_2O_5) and ground in a mortar for 3 h. The homogenized raw materials were pressed into 10 mm×2.5 mm (diameter × height) cylindrical pellets, sintered in a tubular furnace at 5 K/min heating rate, held at 953 K for 2–5 h, and then cooled down slowly to RT.

X-ray diffraction (XRD, Bruker D8 Advance Diffrac-

*Project supported by the National Natural Science Foundation of China (Grant Nos. 11574276, 51702097, and 11574083), the Program for Innovative Research Team (in Science and Technology) in University of Henan Province, China (Grant No. 16IRTSTHN017), and Henan Science and Technology Development Project, China (Grant No. 182102210241).

†Corresponding author. E-mail: liuxiansheng69@126.com
‡Corresponding author. E-mail: yuanbaohe@ncwu.edu.cn

© 2019 Chinese Physical Society and IOP Publishing Ltd

tometer) was used to analyze the crystal phase of the sample. Microstructures were checked using scanning electron microscopy (SEM, JSM-6700 F) and elements were analyzed with energy dispersive spectrum (EDS). Pellet electrical conductivity was measured after polishing and coating both surfaces with Ag paste. Complex impedance was measured using a frequency response analyzer (1 Hz to 4 MHz) in the temperature range from RT to 623 K. The linear thermal expansion coefficients were measured on dilatometers (LINSEIS DIL L75), with heating and cooling rates of 5 K/min.

3. Results and discussion

Figure 1(a) shows the temperature dependent XRD patterns of $Zr_{0.1}Fe_{0.9}V_{1.1}Mo_{0.9}O_7$ from RT to 873 K. The lattice parameters of $Zr_{0.1}Fe_{0.9}V_{1.1}Mo_{0.9}O_7$ are calculated using the least-square method with PowderX program,[20] which decrease with increasing temperature (Fig. 1(b)). The detailed linear coefficients of thermal expansion of $Zr_{0.1}Fe_{0.9}V_{1.1}Mo_{0.9}O_7$ along the a, b, and c axes are -0.4×10^{-6} K^{-1}, -0.97×10^{-6} K^{-1}, and -1.22×10^{-6} K^{-1}, respectively (RT–873 K). However, by the dilatometer measurement, the coefficient of thermal expansion of $Zr_{0.1}Fe_{0.9}V_{1.1}Mo_{0.9}O_7$ is determined to be 0.72×10^{-6} K^{-1} from 140 K to 673 K (Fig. 1(c)). The different results from temperature dependent XRD and dilatometer measurement could relate to the microstructure and thermal hysteresis of ceramics $Zr_{0.1}Fe_{0.9}V_{1.1}Mo_{0.9}O_7$. The sample for temperature dependent XRD is much smaller than that for dilatometer. The XRD measurement begins after holding temperature for 5 min. However, the dilatometer measurement is continuous with temperature.

Figures 1(d)–1(f) show the SEM images and EDS of $Fe_{0.9}Zr_{0.1}V_{1.1}Mo_{0.9}O_7$, respectively. The microstructure presents irregular particles and tiny pores. The pores could result in the above different coefficients. The EDS shows that the elements in the sample include Zr, Fe, Mo, V, and O. From the EDS, the atomic percentages of Zr, Fe, Mo, V, and O in the sample are 1.10%, 8.60%, 10.02%, 14.31%, and 67.97%, respectively, which indicate that the atomic ratio of Zr, Fe, Mo, V, and O is close to 1 : 9 : 9 : 11 : 70.

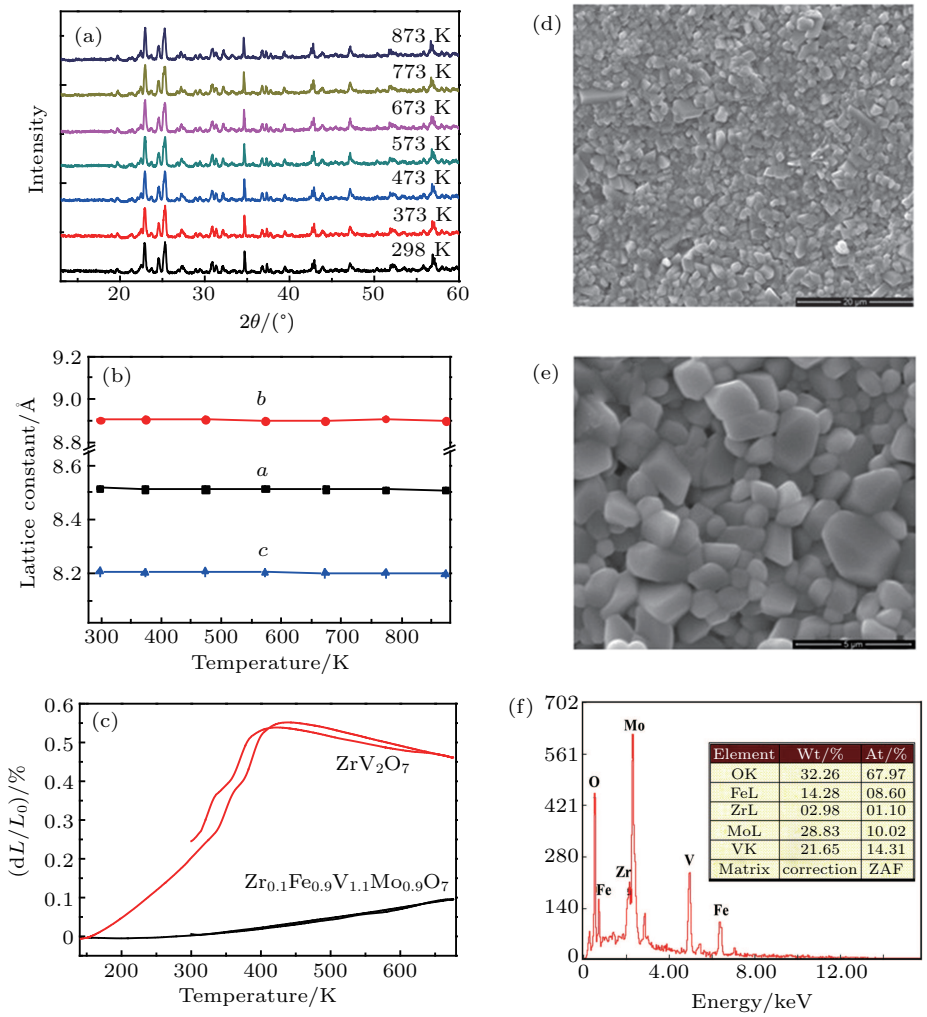


Fig. 1. (a) XRD patterns of $Fe_{0.9}Zr_{0.1}V_{1.1}Mo_{0.9}O_7$ heated from RT to 873 K. (b) Dependence of lattice constants on temperature of orthorhombic $Zr_{0.1}Fe_{0.9}V_{1.1}Mo_{0.9}O_7$. (c) Relative length change of ZrV_2O_7 and $Zr_{0.1}Fe_{0.9}V_{1.1}Mo_{0.9}O_7$ from 140 K to 673 K. (d), (e) SEM images and (f) EDS of orthorhombic $Zr_{0.1}Fe_{0.9}V_{1.1}Mo_{0.9}O_7$.

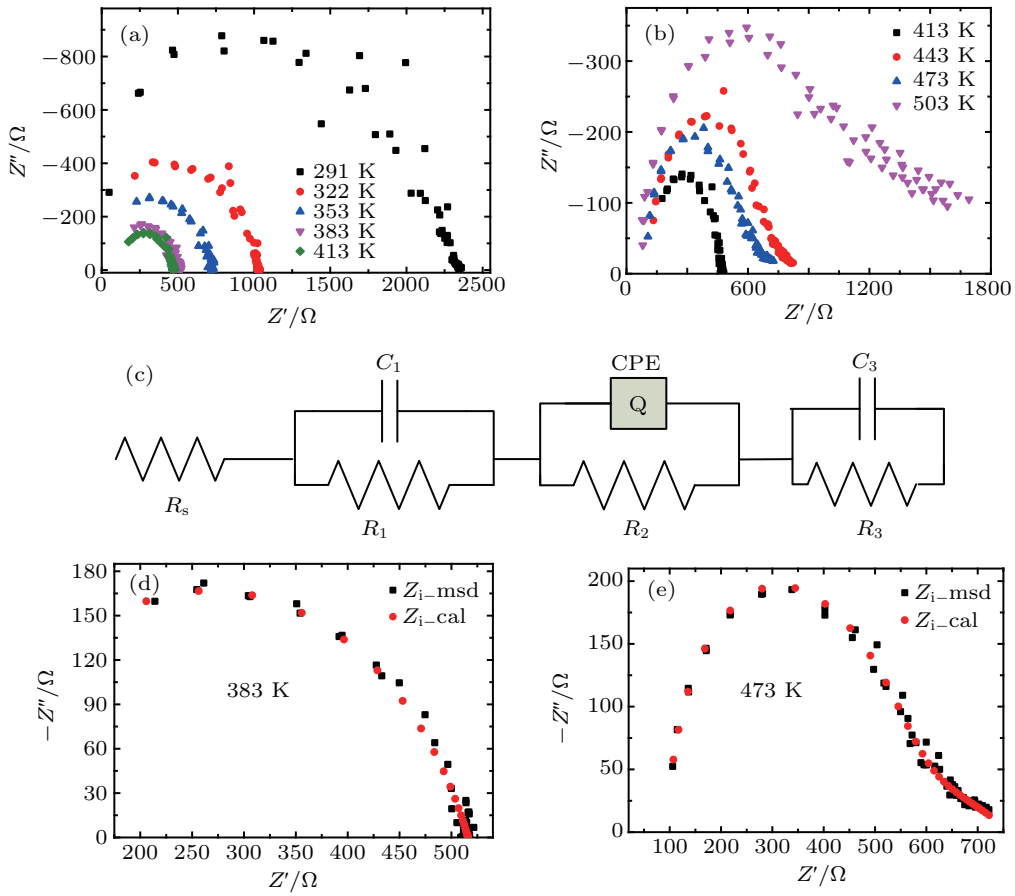


Fig. 2. Representative $Zr_{0.1}Fe_{0.9}V_{1.1}Mo_{0.9}O_7$ AC impedance spectra for (a) 291–413 K and (b) 413–473 K. (c) Equivalent circuit: R_s, R_1, R_2, and R_3 are the electrical resistances of grain, grain boundary, and ion/electrode interface, respectively. Impedance spectra at 383 K (d) and 503 K (e).

Figure 2(a) shows the impedance of $Fe_{0.9}Zr_{0.1}V_{1.1}Mo_{0.9}O_7$ from 291 K to 413 K. The Nyquist plots present a series of arc, where the real axis (Z) corresponds to the contact resistance. With increasing temperature, the radius of the arc decreases, indicating a decrease of resistance. This is similar to the property of semiconductors due to the increase of carrier concentration with heating. At higher temperatures (413–503 K), the Nyquist plots (Fig. 2(b)) show a single semicircle at high frequency, where the real axis (Z) corresponds to the bulk resistance related to the superposition of grain and grain boundary effects. The Nyquist plots present little tails near low frequency, indicating ionic conductivity. These results are in consistent with the results on other ionic conductor materials.[21–23] The Nyquist plots also suggest the increase of resistance with increasing temperature, just like conductor resistance increases with temperature. We use Zsimwin 3.30 program[24] to study the Nyquist curve after stabilization. The impedance of $Fe_{0.9}Zr_{0.1}V_{1.1}Mo_{0.9}O_7$ is calculated by fitting the experimental data (Figs. 2(d) and 2(e)) to the equivalent circuits comprising of resistances R_i, capacitances C_j, and constant phase element CPE, in series and/or parallel, as shown in Fig. 2(c). The total impedance and admittance are

$$Z = R_s + R_1//C_1 + \mathrm{CPE}//R_2 + C_3//R_3 = Z' + \mathrm{j}Z'', \quad (1)$$

$$Y = Y' + \mathrm{j}Y'' = 1/Z, \quad (2)$$

where

$$Z' = R_s + \frac{R_1}{\omega^2 C_1^2 R_1^2 + 1} + \frac{R_3}{\omega^2 C_3^2 R_3^2 + 1} + (R_2//\mathrm{CPE})_r, \quad (3)$$

$$Z'' = \frac{\omega C_1 R_1^2}{\omega^2 C_1^2 R_1^2 + 1} + \frac{\omega C_3 R_3^2}{\omega^2 C_3^2 R_3^2 + 1} + (R_2//\mathrm{CPE})_i \quad (4)$$

are real and imaginary impedances, respectively.

Figure 3(a) shows the impedance from 503 K to 623 K. The Nyquist plots present a single semicircle at high frequency, and have little tails at low frequency. The impedance of $Fe_{0.9}Zr_{0.1}V_{1.1}Mo_{0.9}O_7$ is calculated by fitting the experimental data (Figs. 3(c)–3(e)) to the equivalent circuits comprising of R_i, C_j, and CPE, in series and/or parallel, as shown in Fig. 3(b). The Nyquist plots show that the total resistance of the material does not change and then decreases as the temperature increases, which could relate to the increase of carrier concentration by intrinsic excitation with heating.

To obtain appropriate resistance dependence on temperature, we measured direct-current (DC) current–voltage (I–V) characteristics of $Zr_{0.1}Fe_{0.9}V_{1.1}Mo_{0.9}O_7$ at different temperatures (Fig. 4). The conductance is calculated using the least square method. The total resistance is calculated by $Z' = R_1 + R_2$. The results are consistent with the impedance spectra.

The conductivity σ can then be calculated from[25]

$$\sigma = d/(RA), \quad (5)$$

where d is the thickness, A is the area of the electrode, and R is the electrical resistance. Figure 5 shows the temperature dependent resistance, conductivity, and total conductivity

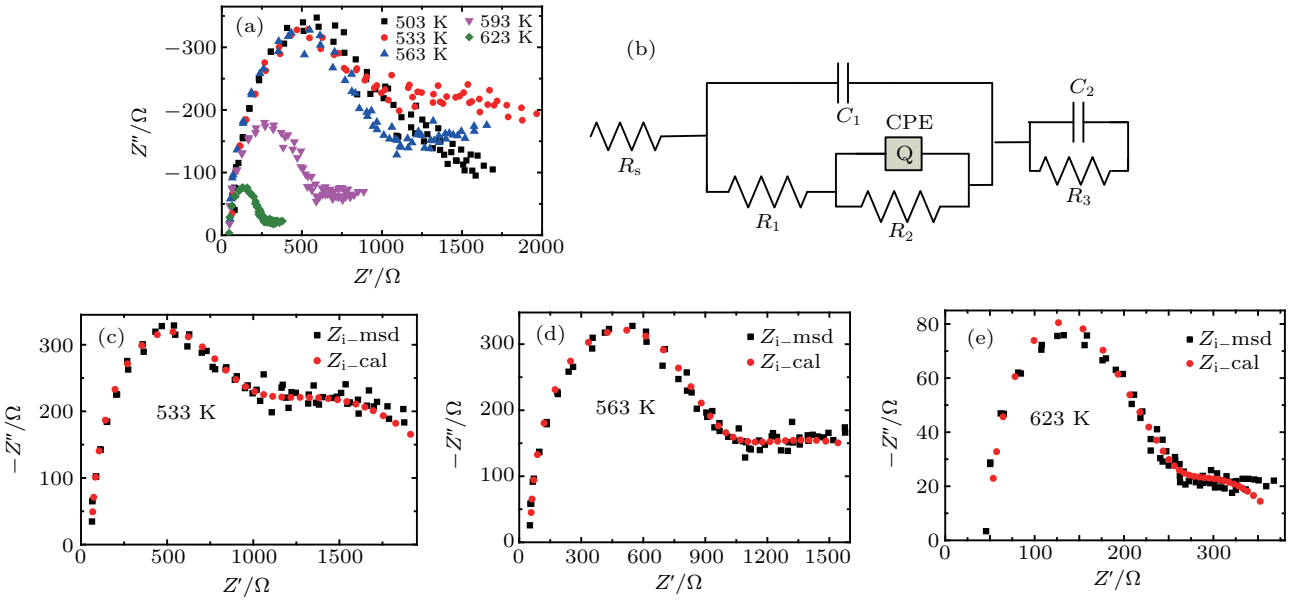


Fig. 3. (a) Representative $Zr_{0.1}Fe_{0.9}V_{1.1}Mo_{0.9}O_7$ AC impedance spectra for 503–623 K. (b) Equivalent circuit: R_s, R_1, R_2, and R_3 are the electrical resistances of grain, grain boundary, and ion/electrode interface, respectively. Impedance spectra at (c) 533 K, (d) 563 K, and (e) 623 K.

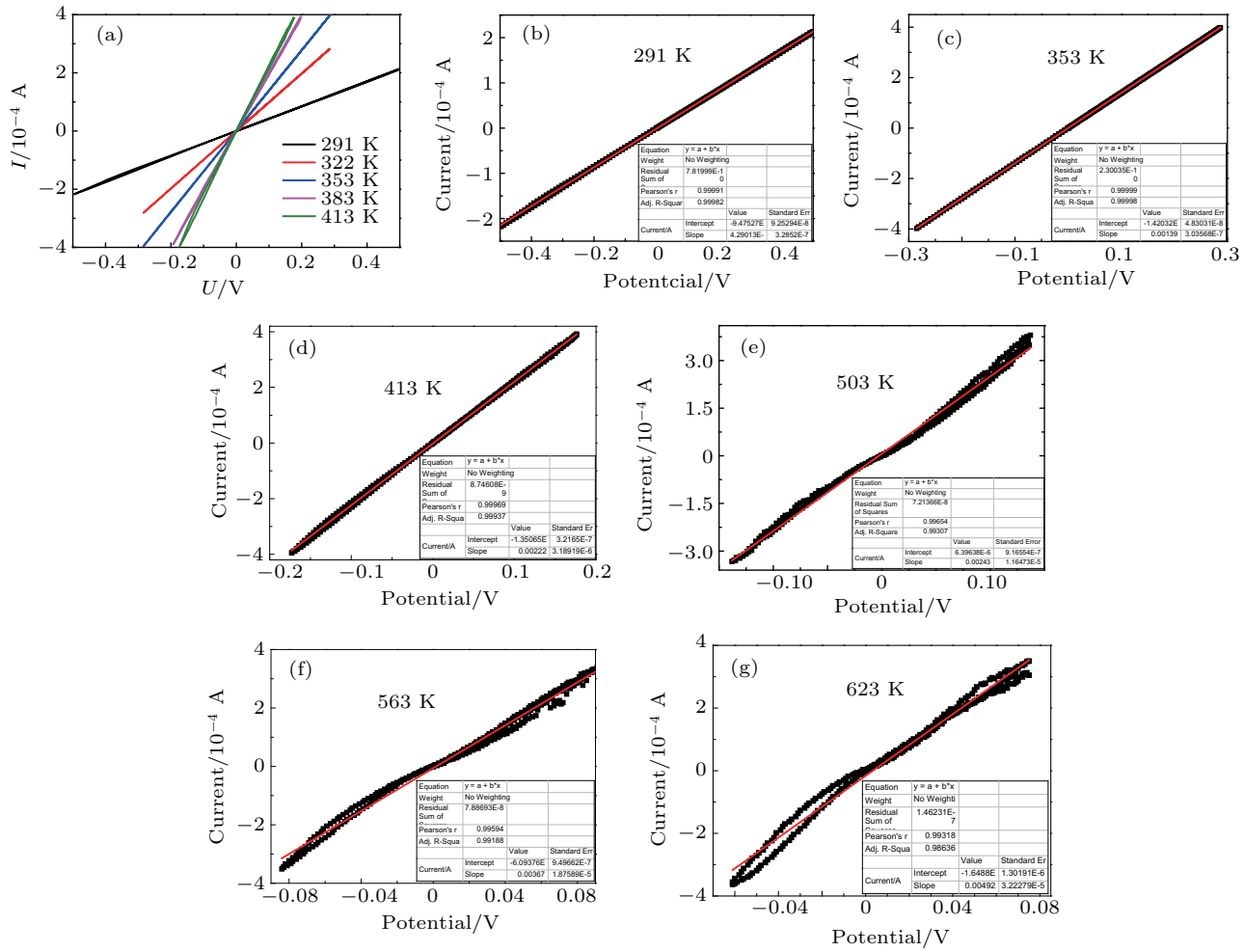


Fig. 4. (a)–(g) The DC I–V curves from 291 K to 623 K of $Zr_{0.1}Fe_{0.9}V_{1.1}Mo_{0.9}O_7$.

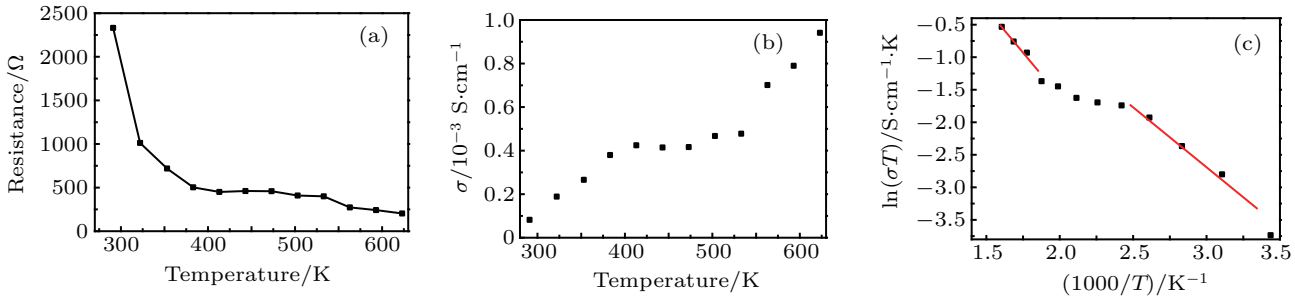


Fig. 5. $Zr_{0.1}Fe_{0.9}V_{1.1}Mo_{0.9}O_7$ total electrical resistance (a) and (b) conductivity, and (c) Arrhenius plots for the total conductivity.

Arrhenius plots for $Zr_{0.1}Fe_{0.9}V_{1.1}Mo_{0.9}O_7$ in normal atmosphere. The values of σ are calculated to be 8.2×10^{-5} S/cm, 3.80×10^{-4} S/cm, 4.16×10^{-4} S/cm, and 9.41×10^{-4} S/cm at 291 K, 383 K, 473 K, and 623 K, respectively. The linear relationship of conductivity with temperature (Fig. 5(c)) could relate to no phase transitions at 291–413 K. The relaxation process activation energy E_a of $Zr_{0.1}Fe_{0.9}V_{1.1}Mo_{0.9}O_7$ at higher temperatures and RT could be calculated to be 0.233 eV and 0.160 eV using Arrhenius expression $\sigma = \frac{\alpha}{T}\exp(-E_a/kT)$, where α is the pre-exponential factor, k is Boltzmann's constant, and T is the absolute temperature.[14]

Carrier concentration could be controlled by temperature.[26–28] The conductivity of $Zr_{0.1}Fe_{0.9}V_{1.1}Mo_{0.9}O_7$ is larger than that of ZrV_2O_7.[14] This could be related to the substituting effect of Fe^{3+}/Mo^{6+} for Zr^{4+}/V^{5+} in ZrV_2O_7, like p type doping ($Fe^{3+} \rightarrow Zr^{4+}$) and n type doping ($Mo^{6+} \rightarrow V^{5+}$) in semiconductor. Fe/Mo co-doping induces the band gap of ZrV_2O_7 to narrow down. Thermal excitation in $Zr_{0.1}Fe_{0.9}V_{1.1}Mo_{0.9}O_7$ (0.160 eV) is easier than that in ZrV_2O_7 (0.319 eV). Meanwhile, the strong interaction between the formed $(Fe_{Zr})^-$ and $(Mo_V)^+$ results in low thermal expansion in $Zr_{0.1}Fe_{0.9}V_{1.1}Mo_{0.9}O_7$. The conductivity presents an obvious change at 413–533 K, which could result from high scattering probability and slowing-down increase of conductive particle number. However, the conductivity increases with increasing temperature (533–623 K), which may be related to the intrinsic thermal excitation of semiconductor.

4. Conclusion

$Zr_{0.1}Fe_{0.9}V_{1.1}Mo_{0.9}O_7$ shows near zero thermal expansion and high conductivity. The conductivities of $Zr_{0.1}Fe_{0.9}V_{1.1}Mo_{0.9}O_7$ are 8.2×10^{-5} S/cm, 3.80×10^{-4} S/cm, 4.16×10^{-4} S/cm, and 9.41×10^{-4} S/cm at 291 K, 383 K, 473 K, and 623 K, respectively. The electrical conductivity is linear for 291–413 K, and the activation energy is 0.160 eV. At 533–623 K, the activation energy is 0.233 eV, indicating that $Zr_{0.1}Fe_{0.9}V_{1.1}Mo_{0.9}O_7$ acts like a classical doped semiconductor. Thermal excitation leads to carrier concentration increase from RT to 413 K, which leads to a rapid resistance decrease. The unchanged conductivity during 413–533 K is due to high scattering probability and slowing-down increase of carrier concentration. The intrinsic thermal excitation leads to rapid increase of conductivity at 533–623 K.

References

[1] Ge X H, Mao Y C, Li L, Li L P, Yuan N, Cheng Y G, Guo J, Chao M J and Liang E J 2016 *Chin. Phys. Lett.* **33** 046503
[2] Liang Y, Cheng Y G, Ge X H, Yuan B H, Guo J, Sun Q and Liang E J 2017 *Chin. Phys. B* **26** 106501
[3] Wang W L, Meng L J, Li L H, Hu L, Zhou K, Kong Z H and Wei B B 2016 *Chin. Phys. Lett.* **33** 116102
[4] Huang R J, Wu Z X, Chu X X, Yang H H, Chen Z and Li L F 2010 *Solid State Sci.* **12** 1977
[5] Chen D X, Yuan B H, Cheng Y G, Ge X H, Jia Y and Liang E J 2016 *Phys. Lett. A* **380** 4070
[6] Yanase I, Sakai H and Kobayashi H 2017 *Mater. Lett.* **207** 221
[7] Chen J, Wang F F, Huang Q Z, Hu L, Song X P, Deng J X, Yu R B and Xing X R 2013 *Sci. Rep.* **3** 2458
[8] Yao W J, Jiang X X, Huang R J, Li W, Huang C J, Lin Z S, Li L F and Chen C T 2014 *Chem. Commun.* **50** 13499
[9] Withers R L, Evans J S O, Hanson J and Sleight A W 1998 *J. Solid State Chem.* **137** 161
[10] Yuan H L, Yuan B H, Li F and Liang E J 2012 *Acta Phys. Sin.* **61** 226502 (in Chinese)
[11] Sahoo P P, Sumithra S, Madras G and Row T N G 2011 *Inorg. Chem.* **50** 8774
[12] Liu Q Q, Yang J, Sun X J, Cheng X N, Tang H and Li H H 2014 *Appl. Surf. Sci.* **313** 41
[13] Yuan B H, Yuan H L, Song W B, Liu X S, Cheng Y G, Chao M J and Liang E J 2014 *Chin. Phys. Lett.* **31** 076501
[14] Yuan B H, Liu X S, Song W B, Cheng Y G, Liang E J and Chao M J 2014 *Phys. Lett. A* **378** 3397
[15] Yuan B H, Liu X S, Mao Y C, Wang J Q, Guo J, Cheng Y G, Song W B, Liang E J and Chao M J 2016 *Mater. Chem. Phys.* **170** 162
[16] Yuan B H, Cao W S, Ge X H, Cheng Y G, Liu X S and Liang E J 2017 *Acta Phys. Sin.* **66** 076501 (in Chinese)
[17] Yuan B H, He X K, Chen L L, Wang W S, Cheng T and Liang E J 2018 *Ceram. Int.* **44** 21621
[18] Nakajima T, Isobe M, Tsuchiya T, Ueda Y and Manabe T 2010 *J. Phys. Chem. C* **114** 5160
[19] Elkady M F, Alrafaa M A, El Essawy N A and Beni-seuf U 2014 *J. Appl. Sci.* **3** 229
[20] Dong C, Wu F and Chen H 1999 *J. Appl. Cryst.* **32** 850
[21] Zhou Y K, Adams S, Rao R P, Edwards D D, Neiman A and Pestereva N 2008 *Chem. Mater.* **20** 6335
[22] Suzuki T and Omote A 2004 *J. Am. Ceram. Soc.* **87** 1365
[23] Omote A, Yotsuhashi S, Zenitani Y and Yamada Y 2011 *J. Am. Ceram. Soc.* **94** 2285
[24] Yu J M, Chao M J, Li D C and Li M Y 2013 *J. Power Sources* **226** 334
[25] Tripathy A, Das S N, Pradan S K, Bhuuan S and Choudhary R N P 2018 *J. Mater. Sci. Mater. Electron.* **29** 4770
[26] Hsu K Y, Wang C Y and Liu C P 2010 *J. Electron. Soc.* **157** K109
[27] Ye C, Fang X, Wang M and Zhang L 2006 *J. Appl. Phys.* **99** 063504
[28] Pejova B, Abay B and Bineva I 2010 *J. Phys. Chem. C* **114** 15280